Hydroxytriazole derivatives as potent and selective aldo-keto reductase 1C3 (AKR1C3) inhibitors discovered by bioisosteric scaffold hopping approach

(Article begins on next page)

14 October 2023

The publisher's version is available at:
http://linkinghub.elsevier.com/retrieve/pii/S0223523417306578

When citing, please refer to the published version.

Link to this full text:
http://hdl.handle.net/2318/1648089

iris - AperTO

Hydroxytriazole Derivatives as Potent and Selective Aldo-keto Reductase 1C3 Inhibitors Discovered by Bioisosteric Scaffold Hopping Approach

Agnese C. Pippione,[1] Alessandro Giraudo,[1] Davide Bonanni,[1] Irene M. Carnovale,[1] Elisabetta Marini,[1] Clara Cena,[1] Annalisa Costale,[1] Daniele Zonari,[1] Klaus Pors,[2] Maria Sadiq,[2] Donatella Boschi,[1] Simonetta Oliaro-Bosso[1]* and Marco L. Lolli.[1]*

[1] *Department of Science and Drug Technology*, University of Torino, via Pietro Giuria 9, 10125 Torino (Italy).
[2] *Institute of Cancer Therapeutics*, Faculty of Life Sciences, University of Bradford, West Yorkshire BD7 1DP (UK).

Abstract

The aldo-keto reductase 1C3 isoform (AKR1C3) plays a vital role in the biosynthesis of androgens, making this enzyme an attractive target for castration-resistant prostate cancer therapy. Although AKR1C3 is a promising drug target, no AKR1C3-targeted agent has to date been approved for clinical use. Flufenamic acid, a non-steroidal anti-inflammatory drug, is known to potently inhibit AKR1C3 in a non-selective manner as COX off-target effects are also observed. To diminish off-target effects, we have applied a scaffold hopping strategy replacing the benzoic acid moiety of flufenamic acid with an acidic hydroxyazolecarbonylic scaffold. In particular, differently *N*-substituted hydroxylated triazoles were designed to simultaneously interact with both subpockets 1 and 2 in the active site of AKR1C3, larger for AKR1C3 than other AKR1Cs isoforms. Through computational design and iterative rounds of synthesis and biological evaluation, novel compounds are reported, sharing high selectivity (up to 230-fold) for AKR1C3 over 1C2 isoform and minimal COX1 and COX2 off-target inhibition. A docking study of compound **8**, the most interesting compound of the series, suggested that its methoxybenzyl substitution has the ability to fit inside subpocket 2, being involved in π-π staking interaction with Trp227 (partial overlapping) and in a T-shape π-π staking with Trp86. This compound was also shown to diminish testosterone production in the AKR1C3-expressing 22RV1 prostate cancer cell line while synergistic effect was observed when **8** was administered in combination with abiraterone or enzalutamide.

1. Introduction

Prostate cancer (PCa) is the most commonly diagnosed cancer and the second leading cause of death in men.[1] Individuals diagnosed with high-risk PCa are typically treated with surgery or a combination of radiation and androgen deprivation therapy (ADT). Many will inevitably relapse and ultimately develop castration-resistant prostate cancer (CRPC), which is responsible for the vast majority of PCa mortalities. Accordingly, there is an unmet clinical need to develop new therapies for the treatment of CRPC patients. Although the mechanisms of resistance are multi-factorial, the androgen axis still plays a major role in being active even after ADT.[2] Beside evidence that androgen receptor (AR) mutations, splice variants and increased copy number represent putative mechanisms of resistance to therapy,[3-6] the increased expression of enzymes able to facilitate the intratumoral conversion of circulating

adrenal androgen precursors to active AR ligands could be responsible of the CRPC surviving mechanisms.[7] In CRPC cells the aldo-keto reductase 1C3 (AKR1C3 or 17β-HSD5) is highly expressed.[5] This enzyme, which catalyzes the reduction of carbonyl substrates derived from both endogenous compounds and xenobiotics,[8] is a key player in several steps of the complex biochemical pathways leading to androgen production of potent AR ligands, as testosterone (T) and 5α-dihydrotestosterone (DHT).[8] Moreover, AKR1C3 has also been discovered to play roles in resistance to both hormone[5] and radiation therapy.[9] Potential clinical use of AKR1C3 inhibitors has been demonstrated as indomethacin (Figure 1), a potent but unselective AKR1C3 inhibitor, is able to circumvent resistance to the steroidogenic enzyme CYP17A1 inhibitor abiraterone,[10] and to the AR antagonist enzalutamide.[11] Few recent studies indicate controversial observations about the *in vivo* effectiveness of AKR1C3-based therapies,[12-14] but other studies strongly indicate AKR1C3 as a therapeutic target in PCa.[3, 15] Although several lead compounds have emerged,[16-19] the *pharmacopeia* still lacks an AKR1C3-targeted drug with clinical potential.
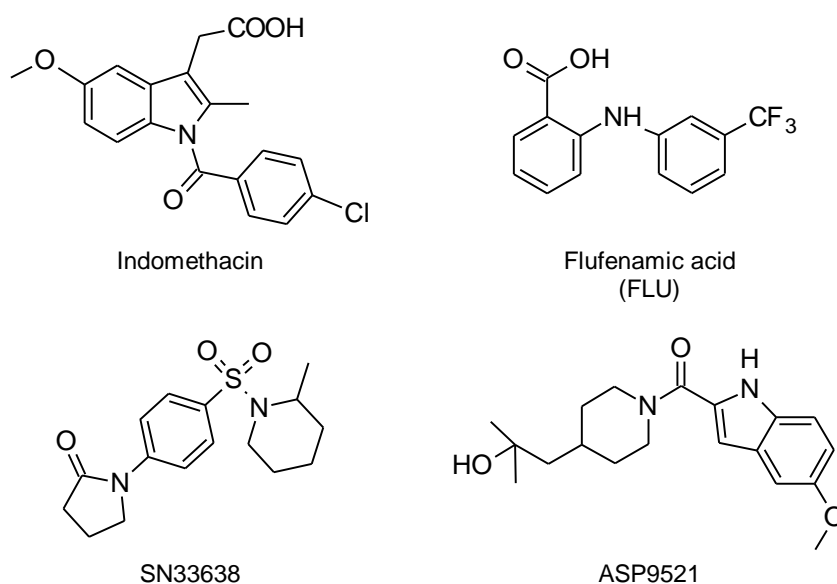
Figure 1. Chemical structures of indomethacin, flufenamic acid and AKR1C3 inhibitors recently deep evaluated.

In order to understand several key unanswered questions related to the *in vivo* application of AKR1C3 inhibitors, it is desirable to develop potent, selective and drug-like AKR1C3 inhibitors. Amongst NSAIDs, flufenamic acid (FLU, Figure 1) potently inhibits AKR1C3 although it suffers from COX off-target effects.[20, 21] Recently, we successfully applied a *scaffold hopping* strategy based on the replacement of quinolinecarboxylate moiety of brequinar with a hydroxyazolecarboxamidic scaffold for the design of new potent human dihydroorotate dehydrogenase (*h*DHODH) inhibitors.[22] In the present study, we applied a similar *scaffold hopping* strategy to the FLU benzoic acid moiety (Figure 2). Specifically, three hydroxyazoles (hydroxyfurazan, hydroxythiadiazole and a series of N-substituted hydroxy-1,2,3-triazoles) were used to design compounds **1 - 8 (**Figure 2). Due to their acidic properties, the hydroxyazole scaffolds are widely deprotonated at physiological pH and are valid isosters of the carboxylic acid function as we recently demonstrated.[23-25] In contrast to the hydroxyfurazan and hydroxythiadiazole scaffolds, the regiosubstitution of the nitrogen of the hydroxytriazole ring allows the possibility to make a structural refinement, which enables an opportunity to improve on binding pocket affinity.[26] Accordingly, the substituents present on the triazole ring (Figure 2) were selected by their possibility of

establishing interactions with sub-pocket 2 (SP2) of the AKR1C3 binding site[27] in an attempt to enhance potency and target selectivity.
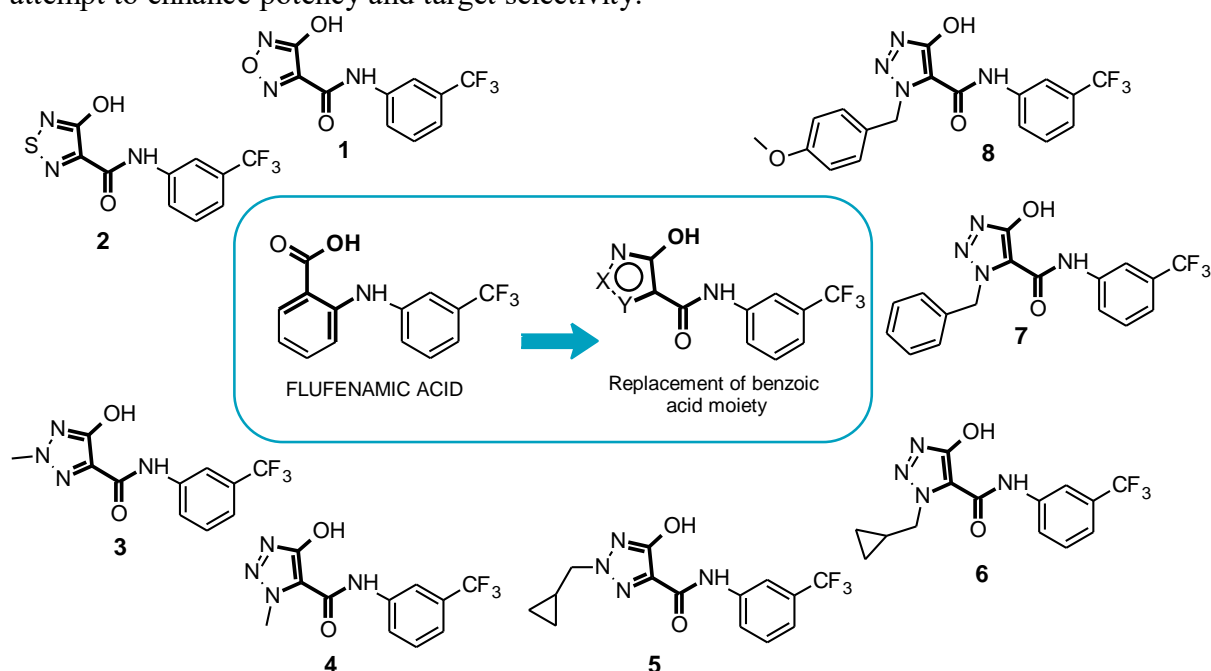
**Figure 2.** AKR1C3 inhibitors based on hydroxyazole scaffolds.

We here report on the design, synthesis and biological explorations of eight candidate structures (Figure 2), which supports the findings of AKR1C3-selective compounds with no off-target COX effect. Furthermore, the binding modes of the most representative molecules were suggested by computational modelling.

2. Result and discussion

2.1 Chemistry.

The methodology used for the synthesis of the target compounds is described in Scheme 1. The first part of the work consisted in acquiring the protected benzyloxyazolecarboxylic acids (compounds **13**, **16 a-f,** Scheme 1a and 1b). Subsequently these acids were coupled with 3-trifluoromethylaniline (Scheme 1c). The furazancarboxylic acid derivative was prepared starting from **9**[25] that was hydrolysed to the corresponding acid **10**. This latter was decarboxylated and dehydrated to the nitrile **11,** then transformed into the methyl ester **12** by a Pinner reaction. Compound **13** was finally obtained by base-catalyzed hydrolysis of **12** (Scheme 1a). Regio-substituted hydroxytriazole carboxylic acids **16 a-f** were prepared from the N-unsubstituted triazole **14** as a common starting material.[23] This building block presents an alkylation pattern directed toward positions $N_{(b)}$ and $N_{(c)}$ of the triazole ring, leading to a mixture of two isomeric products. The isomeric mixtures were chromatographically resolved and each isomer structurally assigned on the basis of the heteronuclear 2D-NMR (HSQC and HMBC) and ^{13}C-NMR spectra.[28] The hydrolysis of the obtained esters **15 a-f** afforded the carboxylic acids of general structure **16** (Scheme 1b). Finally, carboxylic acids **13** and **16 a-f** were converted into the corresponding acyl chlorides and allowed to react with 3-trifluoromethylaniline to generate the amides **18** and **19 a-f** (Scheme 1c); these latter compounds were deprotected through catalytic hydrogenation to give the desired target compounds **1, 3 – 8**. Compound **2** was directly obtained from coupling of unprotected 4-hydroxy-1,2,5-thiadiazole-3-carboxylic acid **17**[29] with 3-trifluoromethylaniline. Although this reaction occured with low yield, the protection of the

hydroxyl group of **17** was avoided as the final removal of benzylic group in oxythiadiazoles is challenging[22].
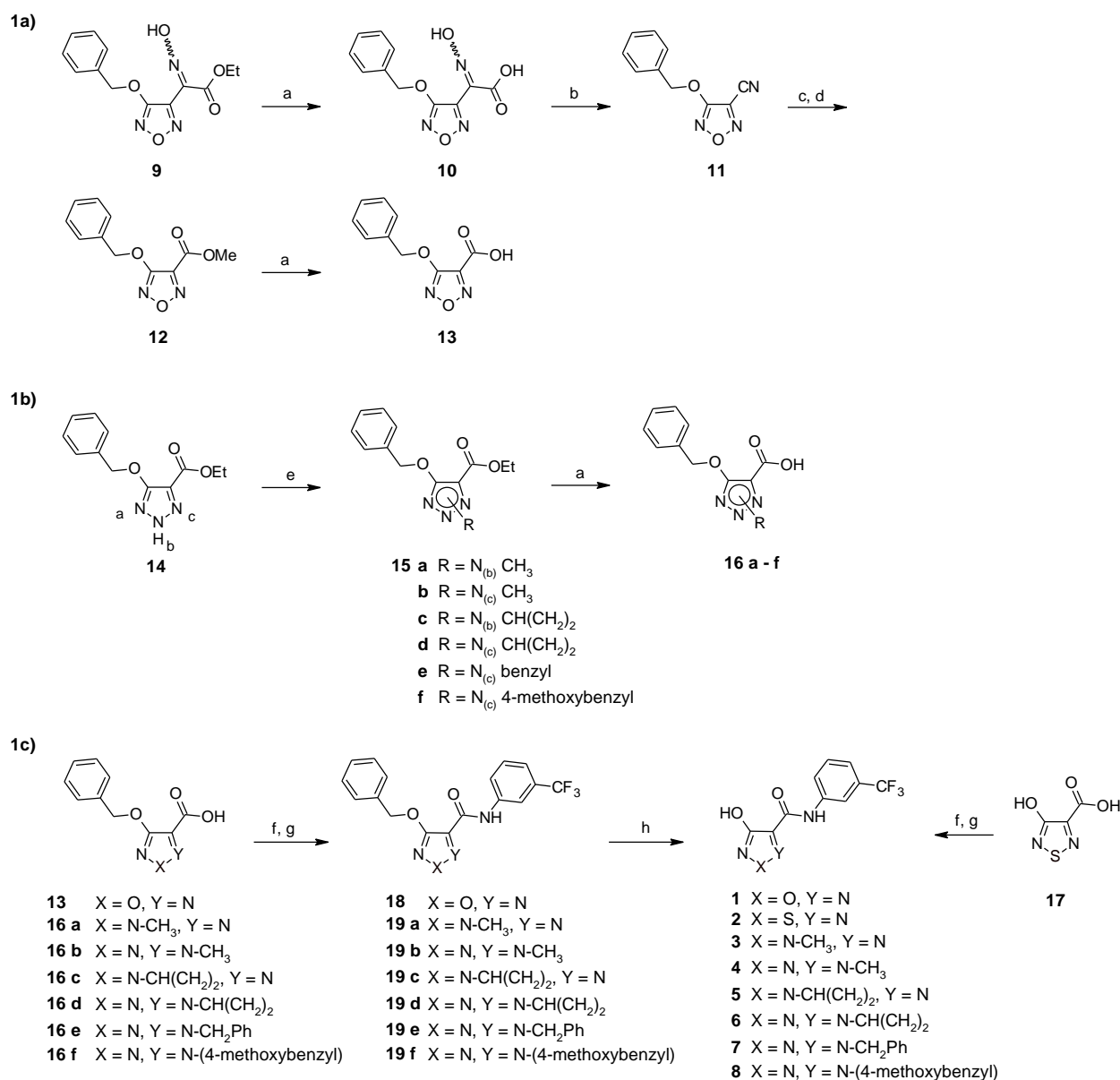
Scheme 1. (a) 1) NaOH, EtOH, rt; 2) 2M HCl; (b) Ac$_2$O, 70°C; (c) NaH, dry MeOH; (d) 2M H$_2$SO$_4$; (e) RX, K$_2$CO$_3$, CH$_3$CN, r.t.; (f) ClCOCOCl, dry DMF, dry THF, 0°C; (g) 3-trifluoromethylaniline, dry pyridine, dry THF, r.t.; (h) H$_2$, Pd/C, THF, r.t.

2.2 AKR1C3 inhibition assays

The activity of the compounds **1** - **8** and FLU as AKR1C3 inhibitors was initially tested by incubating a bacterial suspension containing recombinant AKR1C3 with radiolabeled [^{14}C]-androstenedione in the presence of increasing inhibitor concentrations (Table 1). In comparison with FLU (IC$_{50}$ = 8.63 µM), the hydroxyfurazan **1**, the hydroxythiadiazole **2** and the N(b) methyl triazole **3** were found to be almost inactive while the N(c) methyl triazole **4** (IC$_{50}$ = 32.79 µM) demonstrated weak inhibitory activity. Furthermore, comparing the two cyclopropylmethyl triazoles **5** and **6**, the N(c) isomer resulted in more active compound than the N(b) analogue. As the binding site seems to better tolerate the N(c) substitution, we designed two more N(c) analogues with substituents of increasing size (**7** and **8**). Indeed N(c)

4

cyclopropylmethyl triazole **6** was shown to be more active than N(c) methyl triazole **4,** indicating the preference for lipophilic groups in that position. This hypothesis was confirmed as the benzyl **7** and 4-methoxylbenzyl **8** analogues displayed activity (IC$_{50}$s of 10.19 µM and 3.56 µM, respectively) comparable with FLU. Notably, compound **8** was more potent than FLU under the conditions investigated.

Table 1. Inhibitory effect on AKR1C3 and AKR1C2 recombinant enzymes.

Compound	Bacterial suspension	Purified enzyme		
	AKR1C3 IC$_{50}$ ± SE (µM)[a]	AKR1C3 IC$_{50}$ ± SE (µM)[b]	AKR1C2 IC$_{50}$ ± SE (µM)[b]	Ratio IC$_{50}$ value (1C2:1C3)
FLU	8.63 ± 1.70	0.44 ± 0.02	0.53 ± 0.03	1.2
1	>50 (35.37% ± 3.37)[c]	n.d.	n.d.	n.d.
2	≥ 50 (47.22% ± 3.16)[c]	n.d.	n.d.	n.d.
3	>50 (18.47% ± 3.71)[c]	n.d.	n.d.	n.d.
4	32.79±1.10	n.d.	n.d.	n.d.
5	>50 (5.35% ± 1.44)[c]	n.d.	n.d.	n.d.
6	13.22 ± 0.81	1.60 ± 0.22	70.63 ± 6.32	44
7	10.19±1.47	0.48 ± 0.02	62.94 ± 5.13	131
8	3.56±0.08	0.31 ± 0.01	73.23 ± 8.67	236

a) experiments performed with [^{14}C]androstenedione as substrate; b) experiments performed with S-tetralol as substrate; c) % of inhibition ± SE at 50 µM. n.d: not determined.

The three most active compounds assayed in the bacterial suspension assay (**6 - 8**) were also assayed with AKR1C3 purified enzyme (Table 1) by following the oxidation of S-tetralol in the presence of NADP$^+$. The inhibition pattern observed was similar to that observed with the bacterial suspension. Notably, compounds **7** and **8** were equipotent (IC$_{50}$s 0.48 µM and 0.31 µM, respectively) with FLU (IC$_{50}$ 0.44 µM).

2.3. AKR1Cs selectivity and COX inhibition

In PCa therapy, selective targeting of AKR1C3 over 1C2 is considered critical [30]: AKR1C2 share > 86% sequence identity with AKR1C3, and it is involved in dihydrotestosterone inactivation, so its inhibition would be undesirable. Hence, the most active compounds **6 - 8** and FLU were assayed for their inhibitory properties using purified AKR1C2 incubated with S-tetralol (Table 1). Whereas the AKR1C2/C3 inhibition ratio of FLU was found to be 1.2, triazole analogues **7** and **8** were found to be 131 and 236-fold more

selective toward AKR1C3 inhibition. Next, the compounds **6** - **8** were assayed for their inhibitor effect on COX-1 and COX-2 off-target. Their activity, compared with different standards using ovine COX-1 (*o*COX-1) and human COX-2 (*h*COX-2) is reported in Table 2.

Table 2. COX-1 and COX-2 inhibitory activities of compounds **6**, **7** and **8**, compared with flufenamic acid, indomethacin, celecoxib and rofecoxib.

Compound	*o*COX1 $IC_{50} \pm SE$ (µM)	*h*COX2 $IC_{50} \pm SE$ (µM)	Ratio IC_{50} value (COX1:AKR1C3)	Ratio IC_{50} value (COX2:AKR1C3)
FLU	14 ± 1	> 100 $(18\% \pm 2)^a$	32	> 227
6	> 100 $(17\% \pm 1)^a$	> 100 $(9.6\% \pm 5.2)^a$	> 63	> 63
7	> 100 $(15\% \pm 4)^a$	> 100 $(7.5\% \pm 7.5)^a$	> 208	> 208
8	>100 $(0)^a$	>100 $(12\% \pm 4)^a$	> 322	> 322
Indomethacin	0.10 ± 0.01	0.61 ± 0.09	n.d.	n.d.
Celecoxib	14 ± 12	0.54 ± 0.12	n.d.	n.d.
Rofecoxib	>100 $(25 \pm 14)^a$	3.0 ± 1.0	n.d.	n.d.

a) % of inhibition $\pm$ SE at 100 µM. n.d: not determined.

Notably, compounds **6** - **8** did not display significant inhibitory activity on any of the two COX isoforms at the highest concentration tested (100 µM). In contrast, FLU was shown to be effective in inhibiting COX-1 but not COX-2. Because contradictory data are reported in the literature for FLU and COX inhibition,[31] we validated our assay with indomethacin (time-dependent non-selective inhibitor[31]), celecoxib and rofecoxib (non-time-dependent for COX-1, time-dependent and selective for COX-2).[32, 33] Pleasingly, the COX 1/2 data obtained was consistent with inhibitory potencies reported in literature.[34, 35]

2.4 Antiproliferative activity and testosterone suppression

We evaluated compounds **7**, **8** and FLU in AKR1C3-expressing 22RV1 cells, which have been shown to possess resistance to abiraterone and enzalutamide.[10-12] The presence of AKR1C3 was confirmed using western blot (Figure 3A) before assessing the antiproliferative activity of the three compounds using the sulforhodamine B assay. Although compounds **7**, **8** and FLU appeared to be equipotent AKR1C3 inhibitors, it was observed that **7** is more antiproliferative (Figure 3B). As AKR1C3 plays a key role in the production of testosterone in the androgen biosynthetic pathway, therapeutic intervention of this pathway is vital to effective treatment outcome. Given that **8** had a higher AKR1C3:AKR1C2 selectivity ratio than **7**, we decided to evaluate the former for its ability to interfere with testosterone formation in a cell-based system. This system constitutes a more physiological environment than a homogenate or purified enzyme. Furthermore, working with intact cells allows to observe if the compounds are able to enter the cells. So, AKR1C3-expressing 22RV1 cells were treated with the compound **8** and androstenedione. The formation of testosterone was

analysed in cell supernatant by ELISA. In the presence of only androstenedione, testosterone production was increased > 200-fold. When cells were pre-treated with **8**, a significant dose-dependent impact on testosterone levels was observed (Figure 3C). Encouragingly a significant decrease in testosterone production was observed at 5 μM and 50 % was inhibited at 100 μM. The lack of complete testosterone inhibition might be due to alternative steroidogenic pathways by-passing AKR1C3 activity and/or the binding efficacy of compound **8** to the target is insufficient to completely abolish testosterone production.

Compound	22RV1 IC$_{50}$ ± SE (μM)
FLU	115.0 ± 5.0
7	67.12 ± 2.47
8	81.40 ± 2.29
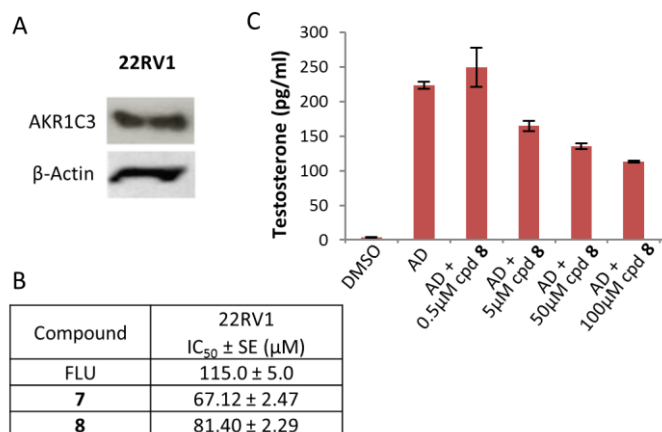
Figure 3. Antiproliferative activity and inhibition of testosterone production, evaluated for representative compounds. Confirmation of AKR1C3 expression in 22RV1 cells by western blot (A) and antiproliferative activity of compounds **7**, **8** and FLU using the SRB assay (B). Inhibitory effect on testosterone production of compound **8** in androstenedione (AD) treated 22RV1 cells (C) by Elisa kit.

In order to evaluate a possible synergistic effect of our compounds with abiraterone and enzalutamide, experiments of co-treatment were performed. 22RV1 cells were treated with 60 μM compound **8** with or without 10 μM abiraterone for 72 h. The same experiment was carried out by treating cells with or without 20 μM enzalutamide. As shown in Figure 4, abiraterone, enzalutamide and compound **8** had limited effects on cell growth. When compound **8** was added together with either abiraterone or enzalutamide, the cell viability was reduced to 45 % or 50 %, respectively, suggesting a synergistic effect was achieved.
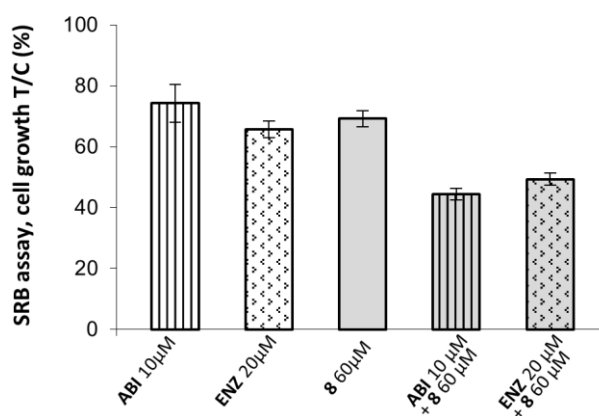
Figure 4. Effect of the co-treatment with compound **8** and abiraterone (ABI) or enzalutamide (ENZ) on 22RV1 cells proliferation by SRB. Cells were treated with 60 μM compound **8** with or without 10 μM abiraterone (or 20 μM enzalutamide) for 72 h. Cell growth is expressed as % T/C (mean OD of treated cells/mean OD of control cells X 100).

2.5 Molecular modeling

To elucidate the observed activity of hydroxytriazole-based compounds, we performed a molecular docking study starting from the crystal structure of the protein complexed with FLU (PDB code: 1S2C).[36] A comparison of compound **8** (grey) and FLU (orange) docked in the AKR1C3 binding site is presented in Figure 5. At first, self-docking procedure was successfully applied on FLU well reproducing the crystallographic pose of FLU inside the binding site (Figure S1). The binding mode of FLU shows the carboxylate moiety interacting with the so-called *oxyanion site* (OS) forming hydrogen bonds with Tyr55, His117 and NADP$^+$ co-factor by a water molecule. The trifluoromethylphenyl moiety is directed toward the SP1, formed by Ser118, Asn167, Phe306, Phe311, Tyr216, Met120 and Tyr319, where it is involved in lipophilic interactions. The docking simulations performed on compound **8** revealed a high superimposition to FLU (Figure S4). In particular, the hydroxyl group present in the triazole ring is located in the OS, thereby mimicking the carboxylic group of FLU. The amide link present in compound **8** compared to the amine in FLU, forces the 3-trifluoromethylphenyl moiety inside SP1. This fact could explain the selectivity of **8** forwards AKR1C3, since the AKR1C2 isoform is characterized by a smaller SP1.[30] Interestingly, the 4-methoxy-benzyl substituent of **8** fits inside SP2, a small pocket part of the steroid channel (SC) left unoccupied by FLU. The docking results suggest the formation of π-π staking and T-shape π-π staking between the N(c) 4-methoxy-benzyl substituent and Trp227 (partial overlapping) and Trp86 respectively.
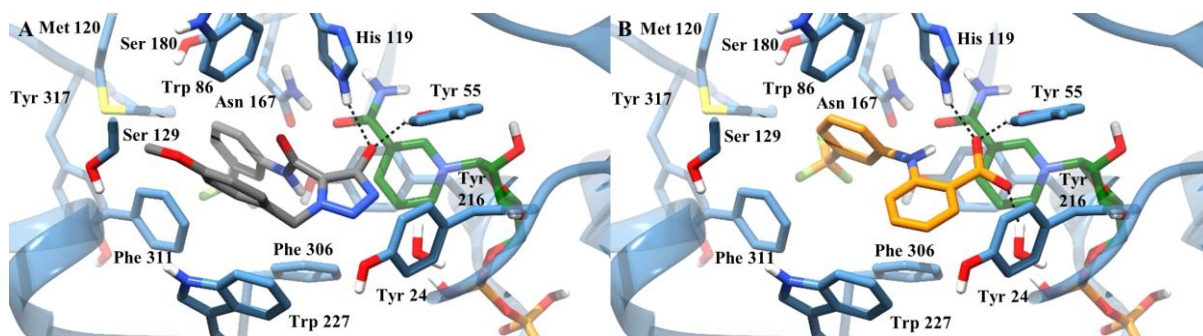
Figure 5. Compound **8** (grey, A) and FLU (orange, B) docked in the AKR1C3 binding site. NADP$^+$ is coloured in green.

We also performed docking simulations using the X-ray structure of COX1 co-crystallized with diclofenac (PDB code: 3N8Y) to clarify the low activity of the compounds versus COX1. The compounds **4**, **6**, **7**, **8** as well as FLU and diclofenac were then docked in the active site (see material and methods for more information). FLU maintained the same interaction of diclofenac, placing the carboxylic portion near Ser530 and Tyr385 and establishing with both residues hydrogen bonds. Moving to compound **4**, this latter was able to mimic diclofenac and FLU binding mode (SP Fig. S5), although associated with a large decrease in binding affinity (SP Tab S1). Instead, a completely different binding mode (data no shown) was found for compounds **6**, **7**, **8**, suggesting that a bulky group in position 1 of hydroxytriazol ring makes the compounds unable to mimic the binding mode of FLU and diclofenac. This modeling analysis shows how the replacement of the FLU benzoic acid by a 4-hydroxy-N1-substituted triazolecarbonylic moiety is a bioisosteric *scaffold-hopping* replacement for AKR1C3 but not for COX1 inhibition activity.

3. Conclusions

This study has focused on a new generation of AKR1C3 inhibitors designed by utilizing a *scaffold hopping* approach to replace the benzoic acid moiety of FLU with hydroxylated azoles. The best compound of the series, the 4-methoxybenzyl substituted analogue **8**, was found to selectively inhibit AKR1C3 activity without any significant AKR1C2 and COX1/2 off-target effects. Compound **8** was also able to inhibit the testosterone production and cell proliferation in AKR1C3-expressing 22RV1 CRPC cells. In addition, the inhibition of AKR1C3 activity by compound **8** partly resensitized 22RV1 cells to enzalutamide and abiraterone treatment. Taken together, the novel chemical scaffolds provides a promising starting point for the design of more potent AKR1C3 inhibitors with clinical potential.

4. Experimental section

4.1 Chemistry

4.1.1 General methods. All chemical reagents were obtained from commercial sources (Sigma Aldrich, Alfa Aesar) and used without further purification. Culture media were obtained from Sigma‑Aldrich. Restriction enzymes, DNA polymerase and T4 DNA ligase were obtained from Promega. [4-^{14}C]-androst-4-ene-3,17-dione (10 μCi/370 KBq, 53.6 mCi/mmol) was obtained from Perkin-Elmer. Analytical grade solvents (acetonitrile, diisopropyl ether, diethyl ether, dichloromethane [DCM], dimethylformamide [DMF], ethanol 99.8 % v/v, ethyl acetate, methanol [MeOH], petroleum ether b.p. 40 - 60°C [petroleum ether]) were used without further purification. When needed, solvents were dried on 4 Å molecular sieves. Tetrahydrofuran (THF) was distilled immediately prior to use from Na and benzophenone under N_2. Thin layer chromatography (TLC) on silica gel was carried out on 5 x 20 cm plates with 0.25 mm layer thickness to monitor the process of reactions. Anhydrous $MgSO_4$ was used as a drying agent for the organic phases. Purification of compounds was achieved with flash column chromatography on silica gel (Merck Kieselgel 60, 230-400 mesh ASTM) using the eluents indicated or by CombiFlash Rf 200 (Teledyne Isco) with 5–200 mL/min, 200 psi (with automatic injection valve) using RediSep Rf Silica columns (Teledyne Isco) with the eluents indicated. Purity of compounds was measured by HPLC analyses, performed on an UHPLC chromatographic system (Perkin Elmer, Flexar). The analytical column was an UHPLC Acquity CSH Fluoro-Phenyl (2.1x100 mm, 1.7 µm particle size) (Waters). Compounds were dissolved in acetonitrile or methanol, and injected through a 20 µl loop. The mobile phase consisted of acetonitrile / water with 0.1 % trifluoroacetic acid; two gradient profiles of mobile phase were used to assay the purity of each compound. UHPLC analysis were run at flow rates of 0.5 mL/min, and the column effluent was monitored at 215 and 254 nm, referenced against a 360 nm wavelength. Purity of the synthetic intermediates varied between 90 % and 99 % purity. The biological experiments were employed on compounds with a purity of at least 95%. Melting points (m.p.) were measured on a capillary apparatus (Büchi 540) by placing the sample at a temperature 10° C below the m.p. and applying a heating rate of 1° C min^{-1}. All compounds were routinely checked by ^{1}H- and ^{13}C-NMR and mass spectrometry. ^{1}H- and ^{13}C-NMR spectra were performed on a Bruker Avance 300 instrument. For coupling patterns, the following abbreviations are used: br = broad, s = singlet, d = doublet, dd = doublet of doublets, t = triplet, q = quartet, m = multiplet. Chemical shifts (δ) are given in parts per million (ppm). MS spectra were performed on Finnigan-Mat TSQ-700 (70 eV, direct inlet for chemical ionization [CI]) or Waters Micromass ZQ equipped with ESCi source for electrospray ionization mass spectra. Compounds **9**,[25] **15a, 15b, 15e**,[23] **15c, 15d, 16a-d**,[22] **17**[29]were prepared following already described procedures.

4.1.2. 2-[4-(Benzyloxy)-1,2,5-oxadiazol-3-yl](hydroxyimino)acetic acid (**10**). 5M NaOH (8 mL) was added to a solution of **9** (2.21 g, 7.60 mmol) in ethanol (40 ml). The reaction

mixture was stirred at room temperature for 24 h, then concentrated under reduced pressure. The crude material was dissolved in water (15 mL) and acidified with HCl until precipitation of the desired product occurred. The white obtained solid was a mixture of the two geometrical isomers in variable ratio. Yield 76 %. ^{1}H-NMR (300 MHz, most abundant isomer, DMSO-d$_6$): δ 5.32 (s, 2H), 7.29 - 7.32 (m, 5H), 13.59 (s, 1H), 13.80 (br s, 1H). ^{13}C-NMR (75 MHz, most abundant isomer, DMSO-d$_6$): δ 74.0, 128.7, 128.8, 128.9, 134.9, 136.5, 139.6, 162.6, 163.3. MS (CI) 263 [M + H]$^+$.

4.1.3. 4-(Benzyloxy)-1,2,5-oxadiazole-3-carbonitrile (**11**). A solution of **10** (1.30 g, 4.94 mmol) in acetic anhydride (13 mL) was stirred at 70 °C for 2 h. The reaction mixture was cooled to r.t. and concentrated under reduced pressure to half volume, then poured into iced water (50 mL). The resulting mixture was stirred at room temperature for 30 min, then extracted twice with diethyl ether. The organic layers were washed with saturated NaHCO$_3$ and brine, dried with Na$_2$SO$_4$ and concentrated under reduced pressure. The oily crude was purified by flash chromatography using DCM as eluent to afford the title compound as a white solid (amorphous solid, m.p. 44.0 – 45.7 °C). Yield 92 %. ^{1}H-NMR (300 MHz, CDCl$_3$): δ 5.35 (s, 2H), 7.34 - 7.42 (m, 5H). ^{13}C-NMR (75 MHz, CDCl$_3$): δ 75.7, 106.3, 125.9, 129.0, 129.1, 129.8, 133.2, 164.6. MS (CI) 202 [M + H]$^+$.

4.1.4. Methyl 4-(benzyloxy)-1,2,5-oxadiazole-3-carboxylate (**12**). Sodium hydride 60 % dispersion in mineral oil (398 mg) was added to a solution of **11** (1.00 g, 4.98 mmol) in dry methanol (10 mL). The reaction mixture was stirred under nitrogen atmosphere at 0 °C for 15 min, then allowed to reach room temperature and further stirred for 60 min. 2M H$_2$SO$_4$ (10 ml) was slowly added cooling the reaction mixture at 0 °C. The resulting suspension was extracted with DCM. The organic layers were collected, dried with brine and Na$_2$SO$_4$ and concentrated under reduced pressure. The crude material was purified by flash chromatography using petroleum ether / DCM 60:40 v/v as eluent, to afford the title compound as a white solid (amorphous solid, m.p. 45 - 48 °C). Yield 98 %. ^{1}H-NMR (300 MHz, CDCl$_3$): δ 3.91 (s, 3H), 5.35 (s, 2H), 7.29-7.43 (m, 5H). ^{13}C-NMR (75 MHz, CDCl$_3$): δ 53.1, 74.4, 128.3, 128.6, 128.9, 134.0, 139.2, 157.4, 163.7. MS (CI) 235 [M + H]$^+$.

4.1.5. Ethyl 4-(benzyloxy)-1-(4-methoxybenzyl)-1H-1,2,3-triazole-5-carboxylate (**15f**). Cs$_2$CO$_3$ (2.90 g, 8.91 mmol) and 1-(chloromethyl)-4-methoxybenzene (1.23 g, 7.94 mmol) were added to a solution of **14** (1.10 g, 4.45 mmol) in CH$_3$CN (25 mL). The resulting mixture was stirred at room temperature for 16 hours. When the reaction was complete, the mixture was concentrated under reduced pressure and the crude product was partitioned between ethyl acetate and water. The aqueous phase was extracted twice with ethyl acetate and collected organic layers were washed with 1M HCl (30 mL), 1M NaOH (30 mL) and brine. The organic phase was dried with Na$_2$SO$_4$ and concentrated under reduced pressure to afford a colorless oil. The latter showed two spots on TLC (eluent: petroleum ether / ethyl acetate 90/10 v/v) relative to the N$_{(b)}$ and N$_{(c)}$ substituted triazole isomers. The two isomers were separated using flash chromatography (eluent: petroleum ether / ethyl acetate 95/5 v/v). First eluted isomer, white solid (powder, m.p. 76.5 - 78.7 °C). Yield 36 %. ^{1}H-NMR (300 MHz, DMSO-d$_6$): δ 1.24 (3H, t, *J* = 7.1 Hz), 3.72 (3H, s), 4.27 (2H, q, *J* = 7.1 Hz), 5.45 (2H, s), 5.73 (2H, s), 6.90 (2H, d, *J* = 8.5 Hz), 7.18 (2H, d, *J* = 8.7 Hz), 7.29 - 7.50 (5H, m); ^{13}C-NMR (75 MHz, DMSO-d$_6$): δ 13.9, 53.5, 55.1, 61.1, 71.1, 110.4, 114.1, 127.5, 127.6, 128.1, 128.4, 129.1, 136.4, 157.7, 159.1, 160.6. MS (ESI) 368 [M + H]$^+$. The second eluted isomer *ethyl 5-(benzyloxy)-2-(4-methoxybenzyl)-2H-1,2,3-triazole-4-carboxylate* was also isolated as a white solid and characterized. M.p. 80.7 – 81.7 °C, from ethanol. Yield 60 %. ^{1}H-NMR (300 MHz, DMSO-d$_6$): *δ* 1.26 (t, *J* = 7.1 Hz, 3H), 3.74 (s, 3H), 4.25 (q, *J* = 7.1 Hz, 2H), 5.30 (s, 2H), 5.48 (s, 2H), 6.92 (d, *J* = 8.6 Hz, 2H), 7.27 (d, *J* = 8.6 Hz, 2H), 7.31 - 7.49 (m, 5H). ^{13}C-NMR (75 MHz, DMSO-d$_6$): *δ* 14.0, 55.0, 58.3, 60.3, 71.7, 113.9, 123.0, 126.7, 127.8, 128.1, 128.3, 129.5, 135.8, 159.1, 159.4, 160.1. MS (ESI) 368 [M + H]$^+$.

*4.1.6. General procedure for compounds **16e, 16f** and **13**.*
6M NaOH (0.57 mL, 3.45 mmol) was added to a solution of the appropriate ester (1.15 mmol) in ethanol (25 mL) and the reaction mixture was stirred at room temperature until disappearance of starting material. The resulting solution was neutralized with 2M HCl, then concentrated under reduced pressure. 2M HCl was added until pH 1-2, observing precipitation of a white solid. The solid was isolated by filtration to give the appropriate carboxylic acid.

4.1.6.1 4-(Benzyloxy)-1,2,5-oxadiazole-3-carboxylic acid (**13**). Crystalline white solid (m.p. 106.1 -107.5 °C from hexane/diisopropyl ether). ^{1}H-NMR (300 MHz, CDCl$_3$): δ 5.45 (s, 2H), 7.30 - 7.50 (m, 5H), 10.91 (br s, 1H). ^{13}C-NMR (75 MHz, CDCl$_3$): δ 74.8, 128.7, 128.8, 129.1, 134.0, 139.1, 161.6, 163.9. MS (CI) 220 [M + H]$^+$.

4.1.6.2 1-Benzyl-4-(benzyloxy)-1H-1,2,3-triazole-5-carboxylic acid (**16e**). Crystalline white solid (m.p. 165.7 - 166.8°C). Yield 90 %. ^{1}H- NMR (300 MHz, DMSO-d$_6$): δ 5.44 (s, 2H), 5.82 (s, 2H), 7.14–7.52 (m, 10H), 13.66 (br, 1H). ^{13}C-NMR (75 MHz, DMSO-d$_6$): δ 53.7, 71.1, 111.2, 127.4, 128.0, 128.1, 128.4, 128.7, 128.7, 135.9, 136.4, 159.1, 160,4. MS (ESI) 310 [M + H]$^+$.

4.1.6.3 4-(Benzyloxy)-1-(4-methoxybenzyl)-1H-1,2,3-triazole-5-carboxylic acid (**16f**). Crystalline white solid (m.p. 179.1 - 180.5°C). Yield 84 %. ^{1}H-NMR (300 MHz, DMSO-d$_6$): δ 3.72 (s, 3H), 5.43 (s, 2H), 5.73 (s, 2H), 6.90 (d, J = 8.3 Hz, 2H), 7.18 (d, J = 8.3 Hz, 2H), 7.29 - 7.51 (m, 5 H), 13.62 (br, 1H). ^{13}C-NMR (75 MHz, DMSO-d$_6$): δ 53.2, 55.1, 71.0, 111.0, 114.0, 127.7, 128.0, 128.1, 128.4, 129.1, 136.4, 159.1, 159.2, 160.5. MS (ESI) 340 [M + H]$^+$.

*4.1.7. General procedure for synthesis of amides **18 - 19a-f**:*
Dry DMF (26 µL) and 2M oxalyl chloride in DCM (3.06 mmol, 1.53 mL) were added to a cooled (0°C) solution of the appropriate carboxylic acid (**13, 16 a - f**, 0.901 mmol) in dry THF (15 mL). The reaction was stirred for 3 hours at room temperature under nitrogen atmosphere. The solvent was evaporated under reduced pressure and the residue was dissolved in dry THF (this process was repeated for three times). The resulting acyl chloride was dissolved in dry THF (10 mL) and used without any further purification in the next step. Dry pyridine (219 µL, 2.70 mmol) and 3-trifluoromethylaniline (113 µL, 0.901 mmol) were added to the described solution. The reaction mixture was stirred for 12 hours at room temperature under nitrogen atmosphere. 0.5 M HCl was added to the resulting mixture, which was concentrated under reduced pressure. The resulting suspension was acidified with 0.5 M HCl to pH 2 and extracted with ethyl acetate (3 × 20 mL). The organic phases were collected, washed with brine, dried with Na$_2$SO$_4$, and the solvent was evaporated. The crude product was purified using flash chromatography (gradient of petroleum ether /ethyl acetate from 90/10 v/v to 70/30 v/v) to obtain the corresponding amide.

4.1.7.1. 4-(Benzyloxy)-N-(3-(trifluoromethyl)phenyl)-1,2,5-oxadiazole-3-carboxamide (**18**). Flash chromatography eluent: petroleum ether / ethyl acetate 9:1 v/v. White solid (powder, m.p. 110.1 - 111.1 °C), yield 74 %. ^{1}H-NMR (300 MHz, CDCl$_3$): δ 5.48 (s, 2H), 7.39-7.52 (7H, m), 7.80 (d, J = 7.6 Hz, 1H), 7.91 (s, 1H), 8.58 (br s, 1H). ^{13}C-NMR (75 MHz, CDCl$_3$): δ 75.2, 116.9 (q, J = 3.8 Hz), 122.0 (q, J = 3.7 Hz), 123.1 (q, J = 0.8 Hz), 123.6 (q, J = 272.6 Hz), 128.7, 128.9, 129.3, 129.9, 131.70 (q, J = 32.1 Hz), 133.9, 137.0, 140.9, 153.8, 163.3. MS (CI) 364 [M + H]$^+$.

4.1.7.2. 5-(Benzyloxy)-2-methyl-N-(3-(trifluoromethyl)phenyl)-2H-1,2,3-triazole-4-carboxamide (**19a**). White solid (powder, m.p. 110.2 - 112.3 °C). Yield 76 %. ^{1}H NMR (300 MHz, DMSO-d$_6$): δ 4.15 (s, 3H), 5.34 (s, 2H), 7.32–7.62 (m, 7H), 8.01 (d, J = 8.2 Hz, 1H),

8.26 (s, 1H), 10.48 (s, 1H). ^{13}C NMR (75 MHz, DMSO-d$_6$): δ 42.4, 72.0, 116.2 (q, J = 4.1 Hz), 119.9 (q, J = 4.1 Hz), 123.6 (q, J = 1.2 Hz), 124.1 (q, J = 272.3 Hz), 125.5, 128.0, 128.2, 128.4, 129.3 (q, J = 31.4 Hz), 129.8, 136.0, 139.4, 158.1, 159.4. MS (ESI) 377 [M + H]$^+$.

4.1.7.3.   4-(Benzyloxy)-1-methyl-N-(3-(trifluoromethyl)phenyl)-1H-1,2,3-triazole-5-carboxamide **(19b).** White solid (powder, m.p. 136.4 - 139.4°C). Yield 58 %. ^{1}H NMR (300 MHz, DMSO-d$_6$): δ 4.20 (s, 3H), 5.52 (s, 2H), 7.31–7.44 (m, 3H), 7.46–7.66 (m, 4H), 7.85 (d, J = 8.2 Hz, 1H), 8.08 (s, 1H), 9.90 (s, 1H). ^{13}C NMR (75 MHz, DMSO-d$_6$): δ 37.9, 71.8, 114.2, 116.1 (q, J =4.1 Hz), 120.6 (q, J = 3.8 Hz), 123.6 (q, J = 1.3 Hz), 123.9 (q, J = 272.3 Hz), 127.9, 128.2, 128.3, 129.5 (q, J = 31.8 Hz), 130.1, 136.2, 138.6, 155.9, 157.8. MS (ESI) 377 [M + H]$^+$.

4.1.7.4.   5-(Benzyloxy)-2-(cyclopropylmethyl)-N-(3-(trifluoromethyl)phenyl)-2H-1,2,3-triazole-4-carboxamide **(19c).** White solid (powder, m.p. 79.0 - 80.7 °C). Yield 75 %. ^{1}H NMR (300 MHz, DMSO-d$_6$): δ 0.41–0.49 (m, 2H), 0.54–0.62 (m, 2H), 1.29–1.42 (m, 1H), 4.25 (d, J = 7.2 Hz, 2H), 5.35 (s, 2H), 7.32 – 7.62 (m, 7H), 8.01 (d, J = 8.2 Hz, 1H), 8.24 (s, 1H), 10.36 (s, 1H). ^{13}C NMR (75 MHz, DMSO-d$_6$): δ 3.6, 10.7, 59.5, 72.0, 116.2 (q, J = 4.3 Hz), 119.9 (q, J = 4.1 Hz), 123.7 (q, J = 0.7 Hz), 124.1 (q, J = 272.4 Hz), 125.6, 128.2, 128.2, 128.4, 129.3 (q, J = 31.3 Hz), 129.8, 136.0, 139.4, 158.1, 159.2. MS (ESI) 417 [M + H]$^+$.

4.1.7.5.   4-(Benzyloxy)-1-(cyclopropylmethyl)-N-(3-(trifluoromethyl)phenyl)-1H-1,2,3-triazole-5-carboxamide **(19d).** White solid (powder, m.p. 114.1 - 116.0 °C). Yield 63 %. ^{1}H NMR (300 MHz, DMSO-d$_6$): δ 0.37 - 0.45 (m, 2H), 0.48 - 0.57 (m, 2H), 1.27 - 1.44 (m, 1H), 4.47 (d, J = 7.3 Hz, 2H), 5.52 (s, 2H), 7.31 - 7.67 (m, 7H), 7.85 (d, J = 8.2 Hz, 1H), 8.08 (s, 1H), 10.06 (s, 1H). ^{13}C NMR (75 MHz, DMSO-d$_6$): δ 3.7, 11.4, 54.9, 71.9, 113.5, 116.1 (q, J = 4.1 Hz), 120.7 (q, J = 4.3 Hz), 123.6 (q, J = 1.2 Hz), 124.0 (q, J = 272.1 Hz), 128.1, 128.3, 128.4, 129.6 (q, J = 31.5 Hz), 130.3, 136.3, 138.7, 156.1, 158.0. MS (ESI) 417 [M + H]$^+$.

4.1.7.6.   1-Benzyl-4-(benzyloxy)-N-(3-(trifluoromethyl)phenyl)-1H-1,2,3-triazole-5-carboxamide **(19e).** White solid (powder, m.p. 152.2 - 154.2 °C). Yield 51 %. ^{1}H NMR (300 MHz, DMSO-d$_6$): δ 5.51 (s, 2H), 5.84 (s, 2H), 7.20 - 7.65 (m, 12H), 7.81 (d, J = 8.1 Hz, 1H), 8.00 (s, 1H), 10.00 (s, 1H). ^{13}C NMR (75 MHz, DMSO-d$_6$): δ 53.4, 72.0, 113. 7, 116.1 (q, J = 3.8 Hz), 120.8 (q, J = 4.3 Hz), 123.6 (q, J = 0.7 Hz), 124.0 (q, J =, 272.3 Hz), 127.7, 128.1, 128.2, 128.4, 128.5, 128.8, 129.6 (q, J = 31.7 Hz), 130.3, 135.7, 136.2, 138.6, 155.9, 158.2. MS (ESI) 453 [M + H]$^+$.

4.1.7.7   4-(Benzyloxy)-1-(4-methoxybenzyl)-N-(3-(trifluoromethyl)phenyl)-1H-1,2,3-triazole-5-carboxamide **(19f).** White solid (powder, m.p. 138.9 - 140.3 °C). Yield 65 %. ^{1}H NMR (300 MHz, DMSO-d$_6$): δ 3.70 (s, 3H), 5.49 (s, 2H), 5.75 (s, 2H), 6.89 (d, J = 7.9 Hz, 2H), 7.24 (d, J = 7.9 Hz, 2H), 7.30–7.67 (m, 7H), 7.82 (d, J = 8.0 Hz, 1H), 8.01 (s, 1H), 10.00 (s, 1H). ^{13}C NMR (75 MHz, DMSO-d$_6$): 52.9, 55.1, 71.9, 113.5, 114.1, 116.1 (q, J = 3.0 Hz), 120.7 (q, J = 3.9 Hz), 123.6 (q, J = 0.5 Hz), 124.0 (q, J = 272.3 Hz) 127.5, 128.1, 128.3, 128.4, 129.5, 129.6 (q, J = 31.8 Hz), 130.3, 136.2, 138.6, 155.9, 158.2, 159.2. MS (ESI) 483 [M + H]$^+$.

4.1.8. General hydrogenation procedure to obtain target compounds **1, 3 - 8.**
The appropriate protected hydroxyazole (**18, 19a-f**, 0.400 mmol) dissolved in dry THF (20 mL) was hydrogenated in presence of Pd/C (45 mg) for 1 hour at atmospheric pressure. The reaction mixture was filtered off through a short layer of celite and the solvent was evaporated under reduced pressure yielding the desired compound.

4.1.8.1. 4-Hydroxy-N-(3-(trifluoromethyl)phenyl)-1,2,5-oxadiazole-3-carboxamide **(1).** White solid (powder, m.p. 165.3 - 167.5 °C, from diisopropyl ether/hexane). Yield 62 %. ^{1}H-NMR

(300 MHz, (CD$_3$)$_2$CO): δ 7.56 (d, J = 7.8 Hz, 1H), 7.69 (t, J = 8.0 Hz, 1H), 8.08 (d, J = 8.1 Hz, 1H), 8.30 (s, 1H), 10.24 (br s, 1H). ^{13}C-NMR (75 MHz, (CD$_3$)$_2$CO): δ 117.8 (q, J = 3.9 Hz), 122.3 (q, J = 3.8 Hz), 124.7, 124.9 (q, J = 272.1 Hz), 131.0, 131.5 (q, J= 32.1 Hz), 139.2, 142.2, 156.7, 163.5. ESI-HRMS (m/z) [M - H]$^-$ calcd. for C$_{10}$H$_5$F$_3$N$_3$O$_3$ 272.0278, obsd. 272.0274.

4.1.8.2. 5-Hydroxy-2-methyl-N-(3-(trifluoromethyl)phenyl)-2H-1,2,3-triazole-4-carboxamide
(3). Crystalline white solid (m.p. 216.6 - 217.0 °C, from acetonitrile). Yield 97 %. ^{1}H NMR (300 MHz, DMSO-d$_6$): δ 4.07 (s, 3H), 7.43 (d, J = 7.8 Hz, 1H), 7.57, (t, J = 8.0 Hz, 1H), 8.00 (d, J = 8.1 Hz, 1H), 8.29 (s, 1H), 10.31 (s, 1H), 11.26 (br, 1H). ^{13}C NMR (75 MHz, DMSO-d$_6$): δ 42.1, 116.2 (q, J = 4.1 Hz), 119.8 (q, J = 3.8 Hz), 123.6 (q, J = 1.1 Hz), 124.2 (q, J = 272.3 Hz), 124.9, 129.4 (q, J = 31.6 Hz), 129.8, 139.5, 158.8, 158.9. ESI-HRMS (m/z) [M - H]$^-$ calcd. for C$_{11}$H$_8$F$_3$N$_4$O$_2$ 285.0605, obsd. 285.0594.

4.1.8.3. 4-Hydroxy-1-methyl-N-(3-(trifluoromethyl)phenyl)-1H-1,2,3-triazole-5-carboxamide
(4). Crystalline white solid (m.p. 235.6 - 241.0 °C, from acetonitrile). Yield 96 %. ^{1}H NMR (300 MHz, DMSO-d$_6$): δ 4.19 (s, 3H), 7.47 (d, J = 7.7 Hz, 1H), 7.59 (t, J = 8.0 Hz, 1H), 7.83 (d, J = 8.2 Hz, 1H), 8.20 (s, 1H), 9.90 (s, 1H), 12.98 (br s, 1H). ^{13}C NMR (DMSO-d$_6$): δ 38.6, 111.9, 116.0 (q, J = 4.1 Hz), 120.3 (q, J = 3.9 Hz), 123.6 (q, J = 1.3 Hz), 124.0 (q, J = 272.4 Hz), 129.6 (q, J = 31.7 Hz), 130.1, 138.8, 156.6, 158.1. ESI-HRMS (m/z) [M - H]$^-$ calcd. for C$_{11}$H$_8$F$_3$N$_4$O$_2$ 285.0605, obsd. 285.0605.

4.1.8.4. 2-(Cyclopropylmethyl)-5-hydroxy-N-(3-(trifluoromethyl)phenyl)-2H-1,2,3-triazole-4-carboxamide **(5).** Crystalline white solid (m.p. 187.3 - 188.4 °C, from acetonitrile). Yield 96 %. ^{1}H NMR (300 MHz, DMSO-d$_6$): δ 0.38 - 0.47 (m, 2H), 0.54 – 0.64 (m, 2H), 1.25–1.40 (m, 1H), 4.18 (d, J = 7.2 Hz, 2H), 7.43 (d, J = 7.8 Hz, 1H), 7.57 (t, J = 8.0 Hz, 1H), 8.01 (d, J = 8.2 Hz, 1H), 8.27 (s, 1H), 10.20 (s, 1H), 11.30 (br, 1H). ^{13}C NMR (75 MHz, DMSO-d$_6$): δ 3.6, 10.7, 59.3, 116.2 (q, J = 3.6 Hz), 119.8 (q, J = 3.7 Hz), 123.7 (q, J = 1.4 Hz), 124.1 (q, J = 272.3 Hz), 124.8, 129.4 (q, J = 31.5 Hz), 129.8, 139.4, 158.6, 159.0. ESI-HRMS (m/z) [M - H]$^-$ calcd. for C$_{14}$H$_{12}$F$_3$N$_4$O$_2$ 325.0910, obsd. 325.0907.

4.1.8.5. 3-(Cyclopropylmethyl)-4-hydroxy-N-(3-(trifluoromethyl)phenyl)-1H-1,2,3-triazole-4-carboxamide (**6**). Crystalline white solid (m.p. 226.9 - 229.0 °C, from acetonitrile). Yield 79 %. ^{1}H NMR (300 MHz, DMSO-d$_6$): δ 0.35 – 0.45 (m, 2H), 0.47 – 0.57 (m, 2H), 1.30 – 1.45 (m, 1H), 4.47 (d, J = 7.3 Hz, 2H), 7.48 (d, J = 7.7 Hz, 1H), 7.60 (t, J = 8.0 Hz, 1H), 7.83 (d, J = 8.2 Hz, 1H), 8.20 (s, 1H), 10.01 (s, 1H), 13.05 (br s, 1H). ^{13}C NMR (75 MHz, DMSO-d$_6$): δ 3.49, 11.2, 55.3, 110.9, 115.9 (q, J = 4.0 Hz), 120.3 (q, J = 3.9 Hz), 123.5 (q, J = 1.1 Hz), 123.9 (q, J = 272.4 Hz), 129.5 (q, J = 31.6 Hz), 130.0, 138.7, 156.5, 158.2. ESI-HRMS (m/z) [M - H]$^-$ calcd. for C$_{14}$H$_{12}$F$_3$N$_4$O$_2$ 325.0907, obsd. 325.0911.

4.1.8.6. 1-Benzyl-4-hydroxy-N-(3-(trifluoromethyl)phenyl)-1H-1,2,3-triazole-5-carboxamide
(**7**). Fluffy white solid (m.p. 222.2 - 224.6 °C, from acetonitrile). Yield 97 %. ^{1}H NMR (300 MHz, DMSO-d$_6$): δ 5.84 (s, 2H), 7.23–7.39 (m, 5 H), 7.46 (d, J = 7.9 Hz, 1H), 7.57 (t, J = 8.0 Hz, 1H), 7.82 (d, J = 8.1 Hz, 1H), 8.13 (s, 1H), 9.88 (s, 1H), 12.73 (br, 1H). ^{13}C NMR (75 MHz, DMSO-d$_6$): δ 53.6, 111.3, 116.2 (q, J = 4.3 Hz), 120.5 (q, J = 4.3 Hz), 123.8 (q, J = 1.3 Hz), 124.1 (q, J = 272.4 Hz), 127.6, 128.1, 128.7, 129.6 (q, J = 31.7 Hz), 130.2, 135.8, 138.7, 156.5, 158.3. ESI-HRMS (m/z) [M - H]$^-$ calcd. for C$_{17}$H$_{12}$F$_3$N$_4$O$_2$ 361.0907, obsd. 361.0908.

4.1.8.7. 4-Hydroxy-1-(4-methoxybenzyl)-N-(3-(trifluoromethyl)phenyl)-1H-1,2,3-triazole-5-carboxamide **(8).** Fluffy white solid (m.p. 215.5 - 217.7 °C, from acetonitrile). Yield 98 %. ^{1}H NMR (300 MHz, DMSO-d$_6$): δ 3.71 (s, 3H), 5.75 (s, 2H), 6.90 (d, J = 8.6 Hz, 2H), 7.25 (d, J = 8.6 Hz, 2H), 7.47 (d, J = 7.8 Hz, 1H), 7.58 (t, J = 7.9 Hz, 1H), 7.83 (d, J =8.2 Hz, 1H), 8.14 (s, 1H), 9.90 (s, 1H), 12.88 (br, 1H). ^{13}C NMR (75 MHz, DMSO-d$_6$): δ 53.2, 55.1,

111.1, 114.1, 116.1 (q, J = 4.1 Hz), 120.5 (q, J = 3.9 Hz), 123.8 (q, J = 1.5 Hz), 124.1 (q, J = 272.1 Hz), 127.6, 129.4, 129.6 (q, J = 30.4 Hz), 130.2, 138.7, 156.5, 158.4, 159.1. ESI-HRMS (m/z) [M - H]⁻ calcd. for $C_{18}H_{14}F_3N_4O_3$ 391.1024, obsd. 391.1031.

4.1.9. 4-Hydroxy-N-[3-(trifluoromethyl)phenyl]-1,2,5-thiadiazole-3-carboxamide (**2**). The compound was obtained following the general procedure for *synthesis of amides* starting from **17**.[29] Flash chromatography eluent: DCM / methanol 90/10 v/v. White solid (powder, m.p. 177.6 – 178.9 °C, from diisopropyl ether). Yield 40 %.¹H-NMR (300 MHz, CD₃OD): δ 7.46 (1H, d, J = 7.9 Hz), 7.56 (1H, t, J = 8.0 Hz), 7.97 (1H, d, J = 8.2 Hz), 8.20 (1H, s). ¹³C-NMR (75 MHz, CD₃OD) δ 118.3 (q, J = 4.0 Hz), 122.3 (q, J = 4.0 Hz), 125.1 (q, J = 1.3 Hz), 125.5 (q, J = 272.5 Hz), 130.8, 132.2 (q, J = 32.3 Hz), 139.7, 140.8, 160.7, 166.0. MS (CI) 290 [M + H]⁺. ESI-HRMS (m/z) [M - H]⁻ calcd. for $C_{10}H_5F_3N_3O_2S$ 288.0049, obsd. 288.0047.

4.2. Expression and purification of recombinant human AKR1C3 and AKR1C2.

Plasmid coding for human AKR1C3 was kindly provided by Prof. J. Adamski (Institute of Experimental Genetics, Genome Analysis Center, Neuherberg, Germany). The cDNA showed one mutation His5Gln in comparison to the NCBI sequence. This conservative mutation is described in the literature as a single nucleotide polymorphism (SNPs) and seems to be very common (refSNP: rs12529). Clone RC213538 containing human AKR1C2 cDNA was obtained by Origene. cDNA was sequenced by the C.R.I.B.I. – BMR Servizio Sequenziamento DNA, Padova (Italy). Then, it was amplified by PCR and, subsequently, subcloned using Xho I and Sal I into the same pGEX 2T- modified plasmid vector (kindly provided by Prof. J. Adamski), used for AKR1C3.
Plasmids coding for AKR1C3 and AKR1C2 were transformed into *Escherichia coli* BL21 (DE) Codon Plus RP (Agilent Technologies). For the protein expression, bacteria cells expressing AKR1C3 and AKR1C2 were grown in YT2X media supplemented with ampicillin at 37 °C with continuous shaking. At OD600 nm = 0.6 the expression was induced by IPTG (0.5 mM). Bacteria were harvested 2 h after induction by centrifugation and stored at -20°C until use. For the AKR1C3 and AKR1C2 purification, bacteria were suspended in PBS supplemented with lysozyme (0.1 mg/ml) and protease inhibitor (Sigma). Then, bacteria were lysed by four freeze-thaw cycles followed by DNA-digestion with benzonase (25 U) in presence of $MgCl_2$ 5 mM. After centrifugation of the lysate for 30 min at 4°C and 13,000 x g, the supernatant was collected. Then, AKR1C3 and AKR1C2 were affinity purified via N-terminal GST-tag on glutathione (GT) sepharose (GE-Healthcare) and cleaved of by thrombin according to the manufacturer's protocol. Expression and purification was monitored by SDS-PAGE.

4.3 In vitro AKR1C3 and AKR1C2 inhibition assays.

The inhibition assays were carried out by using bacterial suspension or purified enzymes. In the screening of AKR1C3 inhibitors, bacteria expressing AKR1C3 were suspended in 100 mM phosphate buffer pH 6.6 without lysis. The bacterial suspension (about 15 μg of proteins) was incubated with [¹⁴C]androstenedione (6 X 10⁻⁴ μCi) in the presence of Tween80 (0.1 mg/mL), ATP (1 mM), $MgCl_2$ (1 mM) and a NADPH generating system (1 mM NADP⁺, 3 mM glucose-6-phosphate and 3 units of G-6-P dehydrogenase) for 30 min at 30°C with vigorous shaking. Inhibitors, when present, were added as solution in ETOH (10% v/v). The enzymatic reaction was stopped by heating at 80 °C for 10 min. After extracting two times with ethyl ether (1.5 mL), the solvent was evaporated and the extract was separated on TLC silica gel plates using chloroform/ethyl acetate (4:1; v/v) as a developing system. Percent conversion of the labeled substrate to testosterone was estimated by integration from

radioactivity scans with a System 200 Imaging Scanner (Hewlett-Packard, Palo Alto, CA, USA).

In order to study the selectivity versus AKR1C2 of the active inhibitors of AKR1C3, the purified recombinant enzymes were used. The activity of the inhibitors was evaluated by using as a substrate S-tetralol in 96-well format. The reaction was fluorimetrically (exc/em; 340 nm/ 460 nm) monitored by the measurement of NADPH production on a "Ensight" plate reader (Perkin Elmer) at 37 °C. Assay mixture contained S-tetralol (in ETOH), inhibitor (in ETOH), 100 mM phosphate buffer, pH 7, 200 µM $NADP^+$, and purified recombinant enzyme (30 µl) in a final volume of 200 µl and 10% ETOH. The S-tetralol concentration used in the AKR1C2 and AKR1C3 inhibition assay were 15 microM and 160 microM, respectively, the some as the Km described for the respective isoforms under the same experimental conditions. Percent inhibition with respect to the controls containing the same amount of solvent, without inhibitor, was calculated from the initial velocities, obtained by linear regression of the progress curve, at different concentrations of inhibitor. The IC_{50} values were obtained using PRISM 7.0, GraphPad Software. The values are the means of two separate experiments each carried out in triplicate.

4.4 COX1 and COX2 inhibition assays

References and selected compounds were tested for their ability to inhibit COX-1 and COX-2 using a COX (ovine/human) Inhibitor Screening Assay Kit (Cayman Chemical Co., Ann Arbor, MI), following manufacturer's instructions. The assay directly measured $PGF_{2\alpha}$ by $SnCl_2$ reduction of COX-derived PGH_2 produced in the COX reaction. The prostanoid product was quantified *via* enzyme immunosorbent assay (ELISA); absorbance measurements were obtained on a PerkinElmer 2030 Multilabel Reader. IC_{50} values were obtained by linear regression using PRISM 7.0, GraphPad Software. Results were calculated as mean value ± standard error (SE) of at least three experiments.

4.5 Tumor cell lines and cell culture.

22RV1 castration-resistant prostate cancer cells were used. Cells were grown in RPMI supplemented with 10% (v/v) fetal calf serum, 2% (v/v) penicillin-streptomycin, 0.03% L-glutamine and maintained at 37 °C in a humidified atmosphere containing 5% CO_2.

4.6 Cell proliferation assay.

Cell growth inhibition was evaluated by sulforhodamine B colorimetric proliferation assay (SRB assay) modified by Vichai and Kirtikara.[37] 22RV1 cells were seeded into 96-well plates in RPMI containing 10% charcoal stripped serum, 2 % (v/v) penicillin-streptomycin and 0.03% L-glutamine, at a density of 10,000 cells/well and incubated at 37 °C with 5% CO_2 for 24 hours to allow cellular adhesion. Various dilutions of inhibitors in ethanol were added in triplicate, and incubated for 72 h. Control cells were incubated with the same final concentration of ethanol (maximum concentration 1% v/v). The assay was done as previously described.[38] For co-treatment experiments, 22RV1 cells were treated with abiraterone (10 µM) or enzalutamide (20 µM) with or without compound 8 (60 µM) for 72 h. The statistical analysis were performed with PRISM 7.0, GraphPad Software. The values are the means of two separate experiments each carried out in triplicate.

4.7 Inhibition of AKR1C3-Mediated Production of Testosterone in 22RV1 cells.

22RV1 cells were seeded into 96-well plates in RPMI media containing 10% charcoal stripped serum, 2% (v/v) penicillin-streptomycin and 0.03% L-glutamine, at a density of 30,000 cells per well, and were incubated at 37°C with 5% CO_2 for 24 hours. Compound **8** was added to the wells at 4 different concentrations and incubated for 1 hour. Equimolar (28nM) concentration of androstenedione was then added to the wells. The plate was returned

to the incubator for a further 24h. Cell supernatant was removed for analysis of testosterone by ELISA following the manufacturer's guide (Testosterone ELISA kit was purchased from Cayman Chemical Company). The ELISA plate was read at a wavelength of 405nM on a microplate reader. Analysis was performed using the Cayman Chemical Company's online available analysis tool and data was quantitated against a standard curve generated in ELISA buffer. Cross reactivity to androstenedione was accounted for by adding these to cell-free wells of the ELISA plate. The statistical analysis were performed with PRISM 7.0, GraphPad Software. The values are the means of two separate experiments each carried out in triplicate.

4.8 Western blot.

25 ug of total protein lysate was loaded for analysis by western blot. For detection of AKR1C3, 1:10,000 dilution of mouse monoclonal anti-AKR1C3 (Sigma Aldrich) was prepared in blocking buffer and added to the membrane with an overnight incubation at 4 °C on a shaker. Mouse B-actin (Sigma Aldrich) was used as internal control with a dilution of 1:20,000 in blocking buffer, with overnight incubation at 4 °C on a shaker. Membranes were subsequently washed with PBST and incubated with secondary goat anti-mouse antibody (Thermo Fisher Scientific) at a dilution of 1:500 for 1 hour at room temperature on a shaker. Membranes were washed and exposed to UV light to detect target bands and captured using a digital camera.

4.9 Molecular Modeling.

The structures of compounds **6, 7** and **8**, as well as the structures of the lead compound Flufenamic Acid, were built in their dissociated forms using the 2D Sketcher tool implemented in Maestro GUI. For each compound, an advanced conformational search was performed using OPLS_2005 as Force Field and setting 1000 maxium steps for each run. Quantum mechanics/molecular mechanics (QM/MM) docking was performed using Schrödinger QM-Polarized Ligand Docking protocol (QPLD).[36] For this purpose, the X-ray crystallographic structure of AKR1C3 was retrieved from RCSB Database (PDB code: 1S2C) and the generated conformers were docked. Before docking, the crystal structure of the protein underwent an optimization process using the Protein Preparation Wizard tool, implemented in Maestro™ GUI. Missing hydrogen atoms were added and bond orders were assigned. Then, DMS, non-structural water molecules and impurities (such as solvent molecules) were removed. The water 2152 was mantained in the binding site because its important water network,[27] also the cofactor NAP and the co-crystalized ligand Flufenamic Acid were maintained. Reorienting automatically optimized the hydrogen bond network: hydroxyl and thiol groups, amide groups of asparagine (Asn) and glutamine (Gln), and the imidazole ring in histidine (His). Moreover, the protonation states prediction of His—aspartic acid (Asp), glutamic acid (Glu), and tautomeric states of His—were accomplished using PROPKA.™ Finally, a restrained minimization of the protein structure was accomplished by converging heavy atoms to a 0.30 Å RMSD. A grid of 10 Å x 10 Å x 10 Å (*x, y,* and *z*) was created and centered on the co-crystalized ligand Flufenamic acid. The ligand was extracted from the structure and used for docking validation. The QPLD protocol was carried out using Glide Extra Precision (XP) mode, setting QM Level to Accurate (B3LYP functional, 6-31G*/LACVP* basis set, ultrafine SCF accuracy level). In the QPLD procedure, after the first XP docking run, QM-derived charge is calculated for the top five poses of each compound in the field of the receptor. Then, a new XP docking is performed with new QM charges calculated. Finally, re-docking and re-scoring were performed, keeping the 10 highest ranked poses. Regarding docking analysis on COX the crystallographic complex of diclofenac and COX1 was used (PDB code: 3N8Y). The same protocol discussed above were utilized for the protein and ligands preparation. The overall of docking were obtained using

Glide XP keeping default parameters and centered the grid on the co-crystalized ligand Diclofenac.

AUTHOR INFORMATION

Corresponding Authors: *
Phone: +39-0116707993. Fax: +39-0116707687, *e*-mail: marco.lolli@unito.it.
Phone: +39-0116706864 . *e*-mail: simona.oliaro@unito.it.
Notes. The authors declare no competing financial interest.

ABBREVIATIONS USED

Aldo-keto reductase 1C3 isoform (AKR1C3), Prostate cancer (PCa), androgen deprivation therapy (ADT), castration-resistant prostate cancer (CRPC), androgen receptor (AR), flufenamic acid (FLU), sub-pocket 2 (SP2), sub-pocket 1 (SP1), cyclooxygenase (COX), aldo-keto reductase 1C2 isoform (AKR1C2), dichloromethane (DCM), dimethylformamide (DMF), methanol (MeOH), Quantum mechanics/molecular mechanics (QM/MM), QM-Polarized Ligand Docking (QPLD), Palladium on carbon (Pd/C), hexadeuterodimethyl sulfoxide (DMSO-d$_6$), deuterochloroform (CDCl$_3$), tetradeuteromethanol (CD$_3$OD), deuterated acetone (CD$_3$)$_2$CO).

ACKNOWLEDGEMENTS

Appendix A. Supplementary data

Supplementary data related to this article can be found at: XXXXXX

References

[1] R.L. Siegel, K.D. Miller, A. Jemal, Cancer statistics, 2016, CA: A Cancer Journal for Clinicians, 66 (2016) 7-30.
[2] Y. Imamura, M.D. Sadar, Androgen receptor targeted therapies in castration-resistant prostate cancer: Bench to clinic, Int. J. Urol., 23 (2016) 654-665.
[3] T. Seisen, M. Roupret, F. Gomez, G.G. Malouf, S.F. Shariat, B. Peyronnet, J.P. Spano, G. Cancel-Tassin, O. Cussenot, A comprehensive review of genomic landscape, biomarkers and treatment sequencing in castration-resistant prostate cancer, Cancer Treat. Rev., 48 (2016) 25-33.
[4] J. Kumagai, J. Hofland, S. Erkens-Schulze, N.F. Dits, J. Steenbergen, G. Jenster, Y. Homma, F.H. de Jong, W.M. van Weerden, Intratumoral conversion of adrenal androgen precursors drives androgen receptor-activated cell growth in prostate cancer more potently than de novo steroidogenesis, The Prostate, 73 (2013) 1636-1650.
[5] T.M. Penning, Mechanisms of drug resistance that target the androgen axis in castration resistant prostate cancer (CRPC), J. Steroid. Biochem. Mol. Biol., 153 (2015) 105-113.

[6] M. Sakai, D.B. Martinez-Arguelles, A.G. Aprikian, A.M. Magliocco, V. Papadopoulos, De novo steroid biosynthesis in human prostate cell lines and biopsies, The Prostate, 76 (2016) 575-587.

[7] W. Zhang, Y. Meng, N. Liu, X.F. Wen, T. Yang, Insights into chemoresistance of Prostate Cancer, Int. J. Biol. Sci., 11 (2015) 1160-1170.

[8] T.M. Penning, The aldo-keto reductases (AKRs): overview, Chem. Biol. Interact., 234 (2015) 236-246.

[9] S.Q. Sun, X. Gu, X.S. Gao, Y. Li, H. Yu, W. Xiong, H. Yu, W. Wang, Y. Li, Y. Teng, D. Zhou, Overexpression of AKR1C3 significantly enhances human prostate cancer cells resistance to radiation, Oncotarget, 7 (2016) 48050-48058.

[10] C. Liu, C.M. Armstrong, W. Lou, A. Lombard, C.P. Evans, A.C. Gao, Inhibition of AKR1C3 activation overcomes resistance to Abiraterone in advanced Prostate Cancer, Mol. Cancer Ther., 16 (2017) 35-44.

[11] C. Liu, W. Lou, Y. Zhu, J.C. Yang, N. Nadiminty, N.W. Gaikwad, C.P. Evans, A.C. Gao, Intracrine androgens and AKR1C3 activation confer resistance to Enzalutamide in Prostate Cancer, Cancer Res., 75 (2015) 1413-1422.

[12] Y.D. Yin, M. Fu, D.G. Brooke, D.M. Heinrich, W.A. Denny, S.M. Jamieson, The Activity of SN33638, an Inhibitor of AKR1C3, on Testosterone and 17beta-Estradiol Production and Function in Castration-Resistant Prostate Cancer and ER-Positive Breast Cancer, Front. Oncol., 4 (2014) 159.

[13] W. Zhou, P. Limonta, AKR1C3 Inhibition therapy in Castration-Resistant Prostate Cancer and Breast Cancer: lessons from responses to SN33638, Front. Oncol., 4 (2014) 162.

[14] Y. Loriot, K. Fizazi, R.J. Jones, J. Van den Brande, R.L. Molife, A. Omlin, N.D. James, E. Baskin-Bey, M. Heeringa, B. Baron, G.M. Holtkamp, T. Ouatas, J.S. De Bono, Safety, tolerability and anti-tumor activity of the androgen biosynthesis inhibitor ASP9521 in patients with metastatic castration-resistant prostate cancer: multi-centre phase I/II study, Invest. New Drugs, 32 (2014) 995-1004.

[15] A. Egan, Y. Dong, H. Zhang, Y. Qi, S.P. Balk, O. Sartor, Castration-resistant prostate cancer: adaptive responses in the androgen axis, Cancer. Treat. Rev., 40 (2014) 426-433.

[16] A. Adeniji, M.J. Uddin, T. Zang, D. Tamae, P. Wangtrakuldee, L.J. Marnett, T.M. Penning, Discovery of (R)-2-(6-Methoxynaphthalen-2-yl)butanoic Acid as a Potent and Selective Aldo-keto Reductase 1C3 Inhibitor, J. Med. Chem., 59 (2016) 7431-7444.

[17] T. Zang, K. Verma, M. Chen, Y. Jin, P.C. Trippier, T.M. Penning, Screening baccharin analogs as selective inhibitors against type 5 17beta-hydroxysteroid dehydrogenase (AKR1C3), Chem. Biol. Interact., 234 (2015) 339-348.

[18] J.U. Flanagan, G.J. Atwell, D.M. Heinrich, D.G. Brooke, S. Silva, L.J. Rigoreau, E. Trivier, A.P. Turnbull, T. Raynham, S.M. Jamieson, W.A. Denny, Morpholylureas are a new class of potent and selective inhibitors of the type 5 17-beta-hydroxysteroid dehydrogenase (AKR1C3), Bioorg. Med. Chem., 22 (2014) 967-977.

[19] A.J. Liedtke, A.O. Adeniji, M. Chen, M.C. Byrns, Y. Jin, D.W. Christianson, L.J. Marnett, T.M. Penning, Development of Potent and Selective Indomethacin Analogues for the Inhibition of AKR1C3 (Type 5 17β-Hydroxysteroid Dehydrogenase/Prostaglandin F Synthase) in Castrate-Resistant Prostate Cancer, J. Med. Chem., 56 (2013) 2429-2446.

[20] T.M. Penning, P. Talalay, Inhibition of a major NAD(P)-linked oxidoreductase from rat liver cytosol by steroidal and nonsteroidal anti-inflammatory agents and by prostaglandins, Proc. Natl. Acad. Sci. U S A., 80 (1983) 4504-4508.

[21] A.O. Adeniji, B.M. Twenter, M.C. Byrns, Y. Jin, M. Chen, J.D. Winkler, T.M. Penning, Development of Potent and Selective Inhibitors of Aldo-Keto Reductase 1C3 (Type 5 17β-Hydroxysteroid Dehydrogenase) Based on N-Phenyl-Aminobenzoates and Their Structure-Activity Relationships, J. Med. Chem., 55 (2012) 2311-2323.

[22] S. Sainas, A.C. Pippione, M. Giorgis, E. Lupino, P. Goyal, C. Ramondetti, B. Buccinna, M. Piccinini, R.C. Braga, C.H. Andrade, M. Andersson, A.C. Moritzer, R. Friemann, S.

Mensa, S. Al-Kadaraghi, D. Boschi, M.L. Lolli, Design, synthesis, biological evaluation and X-ray structural studies of potent human dihydroorotate dehydrogenase inhibitors based on hydroxylated azole scaffolds, Eur. J. Med. Chem., 129 (2017) 287-302.

[23] A.C. Pippione, F. Dosio, A. Ducime, A. Federico, K. Martina, S. Sainas, B. Frolund, M. Gooyit, K.D. Janda, D. Boschi, M.L. Lolli, Substituted 4-hydroxy-1,2,3-triazoles: synthesis, characterization and first drug design applications through bioisosteric modulation and scaffold hopping approaches, Medchemcomm, 6 (2015) 1285-1292.

[24] M.L. Lolli, S.L. Hansen, B. Rolando, B. Nielsen, P. Wellendorph, K. Madsen, O.M. Larsen, U. Kristiansen, R. Fruttero, A. Gasco, T.N. Johansen, Hydroxy-1,2,5-oxadiazolyl moiety as bioisoster of the carboxy function. Synthesis, ionization constants, and pharmacological characterization of γ-aminobutyric acid (GABA) related compounds, J. Med. Chem., 49 (2006) 4442-4446.

[25] M.L. Lolli, C. Giordano, D.S. Pickering, B. Rolando, K.B. Hansen, A. Foti, A. Contreras-Sanz, A. Amir, R. Fruttero, A. Gasco, B. Nielsen, T.N. Johansen, 4-Hydroxy-1,2,5-oxadiazol-3-yl moiety as bioisoster of the carboxy function. Synthesis, ionization constants, and molecular pharmacological characterization at ionotropic glutamate receptors of compounds related to Glutamate and its homologues, J. Med. Chem., 53 (2010) 4110-4118.

[26] M. Lolli, S. Narramore, C.W.G. Fishwick, K. Pors, Refining the chemical toolbox to be fit for educational and practical purpose for drug discovery in the 21st Century, Drug Discovery Today, 20 (2015) 1018-1026.

[27] J.U. Flanagan, Y. Yosaatmadja, R.M. Teague, M.Z.L. Chai, A.P. Turnbull, C.J. Squire, Crystal structures of three classes of non-steroidal anti-inflammatory drugs in complex with aldo-keto reductase 1C3, PLoS One, 7 (2012) e43965.

[28] A. Ducime, New bioisosteric applications of hydroxylated azoles in drug design, PhD Thesis, in: Dipartimento di Scienza e Tecnologia del Farmaco, Turin University, Turin, 2016.

[29] D. Lehmann, R. Eckardt, G. Faust, W. Fiedler, W. Poepel, H.J. Jaensch, H.J. Heidrich, D. Lohmann, Preparation of 3-carboxy-4-hydroxy-1,2,5-thiadiazole as a drug intermediate, in, VEB Arzneimittelwerk, Ger. Dem. Rep. . 1989, pp. 7 pp.

[30] M.C. Byrns, Y. Jin, T.M. Penning, Inhibitors of type 5 17beta-hydroxysteroid dehydrogenase (AKR1C3): overview and structural insights, J. Steroid. Biochem. Mol. Biol., 125 (2011) 95-104.

[31] M. Ouellet, M.D. Percival, Effect of inhibitor time-dependency on selectivity towards cyclooxygenase isoforms, Biochem. J., 306 (Pt 1) (1995) 247-251.

[32] J.K. Gierse, C.M. Koboldt, M.C. Walker, K. Seibert, P.C. Isakson, Kinetic basis for selective inhibition of cyclo-oxygenases, Biochem J, 339 (Pt 3) (1999) 607-614.

[33] C.C. Chan, S. Boyce, C. Brideau, S. Charleson, W. Cromlish, D. Ethier, J. Evans, A.W. Ford-Hutchinson, M.J. Forrest, J.Y. Gauthier, R. Gordon, M. Gresser, J. Guay, S. Kargman, B. Kennedy, Y. Leblanc, S. Leger, J. Mancini, G.P. O'Neill, M. Ouellet, D. Patrick, M.D. Percival, H. Perrier, P. Prasit, I. Rodger, et al., Rofecoxib 4-(4'-methylsulfonylphenyl)-3-phenyl-2-(5H)-furanone]: a potent and orally active cyclooxygenase-2 inhibitor. Pharmacological and biochemical profiles, J. Pharmacol. Exp. Ther., 290 (1999) 551-560.

[34] G. Eren, S. Unlu, M.T. Nunez, L. Labeaga, F. Ledo, A. Entrena, E. Banoglu, G. Costantino, M.F. Sahin, Synthesis, biological evaluation, and docking studies of novel heterocyclic diaryl compounds as selective COX-2 inhibitors, Bioorg. Med. Chem., 18 (2010) 6367-6376.

[35] J.J. Talley, D.L. Brown, J.S. Carter, M.J. Graneto, C.M. Koboldt, J.L. Masferrer, W.E. Perkins, R.S. Rogers, A.F. Shaffer, Y.Y. Zhang, B.S. Zweifel, K. Seibert, 4-[5-Methyl-3-phenylisoxazol-4-yl]- benzenesulfonamide, valdecoxib: a potent and selective inhibitor of COX-2, J. Med. Chem., 43 (2000) 775-777.

[36] S. Schrödinger Suite 2017-1 QM-Polarized Ligand Docking protocol; Glide, LLC, New York, NY, 2017; Jaguar, Schrödinger, LLC, New York, NY, 2017; QSite, Schrödinger, LLC, New York, NY, 2017., in.

[37] V. Vichai, K. Kirtikara, Sulforhodamine B colorimetric assay for cytotoxicity screening, Nat. Protoc., 1 (2006) 1112-1116.

[38] S. Sapino, E. Ugazio, L. Gastaldi, I. Miletto, G. Berlier, D. Zonari, S. Oliaro-Bosso, Mesoporous silica as topical nanocarriers for quercetin: characterization and in vitro studies, Eur. J. Pharm. Biopharm., 89 (2015) 116-125.